Geophysical Research Letters

Supporting Information for

The magnitude and origin of groundwater discharge to eastern U.S. and Gulf of Mexico coastal waters

Kevin. M. Befus[1], Kevin D. Kroeger[2], Chris Smith[3], Peter Swarzenski[4,5]

[1]Civil and Architectural Engineering, University of Wyoming, Laramie, WY 82071
[2]Coastal and Marine Science Center, U.S. Geological Survey, Woods Hole, MA
[3]Coastal and Marine Science Center, U.S. Geological Survey, St. Petersburg, FL
[4]Coastal and Marine Science Center, U.S. Geological Survey, Santa Cruz, CA
[5]International Atomic Energy Agency, Monaco

Contents of this file

Additional Supporting Information

Introduction

The supplemental information contains three sections that extend the discussion of 1) the hydrogeologic frameworks of the model regions, 2) the development and implementation of the numerical model for solving the groundwater flow equation, 3) the differences between this analysis and other coastal groundwater discharge studies, and 4) a summary of model performance and description of supplemental file Model_Performance_Summary.pdf.

Text S1. Regional hydrogeologic frameworks

The goal of the numerical modeling was to incorporate the geologic, hydrologic, and other landscape heterogeneities across spatial and temporal scales that control the magnitude and location of SGD (Figure S1). Where possible, published hydrogeologic framework data from

calibrated groundwater flow models were used to define the hydraulic parameters (i.e., horizontal and vertical hydraulic conductivity, K_h and K_v) and the hydrogeologic units (i.e., number of model layers, thickness, and extent). Given the different sources of hydrogeologic data, each region required additional data processing to prepare the model inputs.

New England hydrogeologic framework

The geologic framework of New England consists primarily of glacially-deposited sediment overlying crystalline bedrock. The aquifers in New England are mostly comprised of glacial sands and gravel sediments (N100GLCIAL) and fractured crystalline bedrock aquifers (N600NECRSN). Effectively, a two layer model was adopted to represent the geologic setting of New England: surficial sediment overlying crystalline bedrock. However, a total of nineteen layers were used to parameterize the geologic structure of the Newark and Hartford Basins and include the stratigraphy of the North Atlantic Coastal Plain aquifer system, which contained 19 layers. Where the geologic framework was comprised of glacial sediment overlying crystalline bedrock, only the uppermost three layers were used: the top layer represented glacial or other sediment, the second layer was initially set to 2 m with a K_h=1 m/day to serve as a buffer between the sediment and crystalline rock and physically could represent fracture bedrock, and the third layer was prescribed as crystalline bedrock extending to at least 100 m below sea-level. Crystalline bedrock horizontal hydraulic conductivity was prescribed as 0.001 m/day [*Gleeson et al.*, 2014]. When not specified by the contributing datasets, the vertical hydraulic conductivity was set at one-tenth of the K_h. The hydraulic conductivity and thickness of the surficial materials were obtained from the 1 km x 1 km hydrogeologic framework for U.S. glacial aquifer system but did not provide any information for Maine and New Jersey [*Bayless et al.*, 2017].

In Maine, derived sediment thicknesses from borehole logs (n=45,932) [*Maine Geological Survey*, 2011] were interpolated into a sediment thickness map. The sediment thickness dataset for Maine was created by calculating the median sediment thickness on a 1 km x 1 km grid for areas defined by unique surficial sediment types [*Soller et al.*, 2012]. A Gaussian filter with a 9 km kernel was then applied for each sediment type to fill in only the cells that did not have nearby data, and the sediment thicknesses for each sediment type were then combined to create the final dataset that was inserted into the glacial materials datasets where no data were originally available. The surficial sediment types were also used to prescribe representative K_h values from smaller-scale models in Maine [*Nielsen and Locke*, 2015].

In New Jersey, borehole data were not readily available, so the sediment thicknesses were prescribed using the mean value for sediment thickness ranges from an older Quaternary sediments dataset [*Soller et al.*, 2012]. Similar to in Maine, these sediment types were also used to estimate the K_h for the surficial materials based on other numerical modeling efforts [*Nielsen and Locke*, 2015] (Figure S2). In addition, a hydrogeologic framework for the Newark Basin was produced using surficial bedrock geology maps and cross-sections [*Schlische*, 1992; *Dalton et al.*, 2014]. Bedrock K_h values were assigned using mean lithology-based parameters [*Gleeson et al.*, 2014].

A hydrogeologic framework for the Hartford Basin was also created using bedrock geology maps and representative cross-sections [*Resor and DeBoer*, 2005; *Gleeson et al.*, 2014] (Figure S2). Bedrock K_h values were also assigned using mean lithology-based parameters [*Gleeson et al.*, 2014].

North Atlantic Coastal Plain hydrogeologic framework

The geologic framework of the North Atlantic Coastal Plain (NACP) aquifer system is comprised of an unconfined surficial aquifer underlain by a sequence of confined aquifers and confining units. The sediment making up these hydrogeologic units were deposited since the early Cretaceous period over multiple cycles of marine transgressions and regressions [*Ator et al.*, 2005]. Crystalline bedrock exists below the NACP aquifer system and becomes shallower inland until it is exposed at the surface, marking the Fall Zone boundary between the crystalline bedrock terrain and the coastal plain regressions [*Ator et al.*, 2005]. East of the Fall Zone, the hydrogeologic framework for the current modeling study were developed from the model 1 mile by 1 mile inputs of Masterson et al. [2016], including model layer thicknesses, K_h, and K_v. West of the Fall Zone was not incorporated into the groundwater flow models. An additional 10-meter thick layer with K_h= 1 m/day and K_v=0.1 m/day was added along the bottom boundary of the model to serve as a thin fractured bedrock unit and to assist with model convergence in areas near the Fall Zone with thin overlying units. Following Masterson et al. [2016], general head boundaries were applied to the seaward edges of model layers that were truncated towards the coast. While Masterson et al. [2016] used an iterative approach to define the freshwater head on these boundary conditions, we approximated the freshwater head assignment by using the depth of the general head boundary cell from sea-level as the saltwater head.

Southeastern Atlantic Coastal Plain hydrogeologic framework

The geologic framework of the Southeastern Atlantic Coastal Plain (SACP) aquifer system consists of an unconfined surficial aquifer underlain by a sequence of confined aquifers and confining units. The SACP region represents the north-south transition between the NACP and Floridan aquifer systems, containing portions of hydrogeologic units from both regions. The hydrogeologic framework of the current study was developed from the 1 mile by 1 mile model inputs of Campbell and Coes [2010] covering the entirety of the SACP region. While the hydrogeologic framework data are available in raster form online (https://water.usgs.gov/ogw/gwrp/activities/gspdata/Studies/NSCCoastal.html), the raster data contained erroneously intersecting geologic units. Model layer thickness, K_h, and K_v were provided by the previously run models [*Campbell and Coes*, 2010], where K_v was calculated from optimizing anisotropy values to match measured head data.

Floridan hydrogeologic framework

The geologic framework of the Floridan region consists of a surficial unconfined aquifer above the mostly semi-confined Floridan carbonate aquifer system overlying additional confined aquifers [*Williams and Kuniansky*, 2016].Published hydrogeologic framework spatial datasets provided the initial data that constrained the model layers and their hydraulic properties [*Williams and Dixon*, 2015]. These data were available in raster (1 km x 1 km resolution) and vector forms that were clipped to the coastline. The Lower Floridan aquifer was the lowest stratigraphic unit used in the development of the model inputs. Vector isopach data were manually extended offshore by linearly extrapolating the contours. Raster hydraulic property data were extended offshore using a Gaussian two-dimensional smoothing filter with a three-cell kernel followed by linear extrapolation. The transmissibility and thickness of the Upper Floridan aquifer was used to calculate K_h and was then used to prescribe the K_h for both the Upper and Lower Floridan aquifers, since no data were available on the Lower Floridan aquifer. A constant anisotropy (K_h/K_v) of 1.3 was used for all model layers [*Williams and Kuniansky*, 2016].

Coastal Lowlands hydrogeologic framework

The geologic framework of the Coastal Lowlands aquifer systems surrounding the Gulf of Mexico are comprised of multiple layers of primarily sandy sediment undergoing burial and diagenesis with interbedded clay units [*Martin Jr. and Whiteman Jr.*, 1999; *Thompson et al.*, 2007]. Isopach data in vector format were manually extended off-shore by linearly extrapolating the contours and then converted into gridded data [*Martin Jr. and Whiteman Jr.*, 1999]. Hydraulic properties were estimated following a previous modeling effort in the central Gulf of Mexico that conceptualized the poorly-constrained interbedded clays as a source of anisotropy integrated over each model layer [*Thompson et al.*, 2007]. Thus, a constant anisotropy of 10 was used for all model layers.

Text S2. Groundwater model and post-processing details

Data inputs. The source datasets varied in the amount of information supplied, with some sources supplying gridded information for all of the parameters and others only providing stratigraphic control with constant hydraulic properties (Table S1). These separate hydrogeologic regions were necessary because no seamless subsurface structure data exist that connect the respective aquifer systems. Thus, each region had an internally continuous geologic framework, but overlapping portions of neighboring regions contain different hydrogeologic structure due to differences between regions in naming and defining hydrogeologic units. A total of 40 overlapping groundwater models were developed for these regions using the same collection of boundary conditions to allow automated model runs using Python and FloPy [*Bakker et al.*, 2016] (Figure S3).

All of the source datasets had coarser cell sizes than the 250 m x 250 m cell size for the models in this analysis, so the gridded input data were first smoothed using a two-dimensional Gaussian filter to remove cell-to-cell edge effects, projected into a consistent geographic coordinate system (Geographic Coordinate System of the North American Datum of 1983, GCS NAD 1983), and then linearly interpolated to the model nodes.

Numerous spatial datasets were required to construct and run the MODFLOW models. The published hydrogeologic framework data comprised the majority of model inputs (Table S1). Additionally, a continuous topography-bathymetry elevation model with 3 arc-second (~90 m) resolution provided the land and ocean surface topography and set the top of the hydrogeologic framework [*Befus and Kroeger*, 2017]. Groundwater recharge was supplied to the models as a prescribed flux using average effective groundwater recharge rates for the 2000-2013 period on a ~800 m grid over the conterminous United States using a joint water budget and statistical analysis product [*Reitz et al.*, 2017]. The input recharge data masked inland waterbodies with no recharge [*Reitz et al.*, 2017], but the higher resolution of our model and difference in model conceptualization (i.e., waterbodies were not modeled separately or assigned as constant head in our models) allowed the potential in our models for recharge to occur in these areas. Therefore, we used a Gaussian filter to fill in these zero recharge areas to 3 km from a non-null value and assigned the nearest recharge value for any remaining zero recharge cells.

Discretization. Model domains were created by fitting the polygon representing the active catchments to model with the smallest bounding rectangle. The bounding rectangle was then projected from the base geographic coordinate system to the nearest Universal Transverse Mercator (UTM) projection and then shifted and rotated to have an origin at (0 m, 0 m). A regular grid was constructed within the rectangle to define the model domain. The

original model-defining polygon was then used to set active and inactive model cells, where cells outside of the polygon were set to inactive. All of the MODFLOW models in this analysis were run with a constant grid cell size of 250 m by 250 m in the x-y dimensions, and the thickness of the cells was prescribed by the input hydrogeologic unit thickness data. Thus, cell thicknesses ranged from a minimum of 0.3048 m to > 1000 m. Minimum cell thicknesses were prescribed per geographic region and varied between 0.3048 m to 2 m.

Each model domain was split into three cell types: inactive no-flow cells outside of the active model domain specified by buffered HUC8 watershed-based domains [*Herrmann et al.*, 2015], marine cells within the active area but with a surface elevation below sea-level (set to ≤ 0 m), and land cells within the active area and above sea-level. While the watershed-based domain set the maximum model extent, hydrogeologic framework data did not always have the same inland boundaries. Where either no hydrostratigraphic data were available (e.g., near Mobile Bay, AL) or major geologic discontinuities inland marked the inland extent of the coastal aquifer system (e.g., the Fall Line marking the western boundary of the Atlantic Coastal Plain), model cells were set to inactive, creating no-flow boundaries.

Recharge-Drain Boundary. All model cells in the topmost layer with an elevation larger than sea-level were prescribed as a combined recharge-drain boundary condition using the MODFLOW Recharge (RCH) and Drain (DRN) packages. This boundary conditions allows recharge to enter the model only if the water table is below the top of the cell, otherwise the cell becomes a discharge location with a flux that depends upon the head in that cell. The surface conductance (m^2/day) was calculated with:

(1)

where Ac_{ell} was the top area of the model cell [m_2], $K_{v,surf}$ was the vertical hydraulic conductivity of the top model cell [m/day], z_{surf} was the elevation of the top of the cell [m], and z_{cc} was the elevation of the center of the cell [m].

General Head Boundary. All model cells in the topmost layer with an elevation lower than sea-level, prescribed in this analysis as 0 m, were assigned to be flux-dependent, general-head boundary conditions using the MODFLOW General Head Boundary package (GHB). The surface conductance (m^2/day) set by:

$$C_{surf} = \frac{A_{cell}\, K_{v,surf}}{z_{bed}} \tag{2}$$

where A_{cell} was the top area of the model cell [m^2], $K_{v,surf}$ was the vertical hydraulic conductivity of seabed materials [m/day], and z_{bed} was the thickness of seabed materials [m]. Seabed materials become more fine-grained offshore, creating a low permeability layer. Therefore, $K_{v,surf}$ was defined to be 100 times smaller than the K_v of the top model layer cells. For all models, z_{bed} was set to a constant 5 m as a representative value for coastal shelves [*Thompson et al.*, 2007]. The boundary head applied to the marine cells was specified as the freshwater head, h_f [m], defined as:

$$h_f = \frac{\rho_i}{\rho_f} h_i - \frac{\rho_i - \rho_f}{\rho_f} z_i \tag{3}$$

where an initial head value, h_i [m], at the original density, ρ_i [kg/m^3], was converted to its equivalent h_f with a freshwater density, ρ_f [kg/m^3]. To assign the boundary heads, the elevation head, z_i, [m], was the depth of seawater at each cell center, h_i as sea-level at 0 m, ρ_f to 1000 kg/m^3, and ρ_i to 1025 kg/m^3. Thus, the h_f defined the hydraulic head that had to be overcome by

groundwater in underlying cells for SGD to occur. The freshwater-saltwater interface was not explicitly or implicitly incorporated into the model, as the solution of the interface position is highly nonlinear and would require significant additional computational resources. No recharge was applied to marine model cells, and the initial head for the marine cells was set to h_f for the top layer and to the elevation at the top of each subsequently lower layer.

The seepage boundary condition (DRN) is a flux-dependent boundary similar to GHB, except that the external pressure head is set to zero (i.e., atmospheric pressure) and no net groundwater flux occurred across the cell top when the head fell below the land surface. Thus, the DRN boundary only allowed groundwater discharge at the surface, whereas the GHB boundaries could experience bi-directional fluxes. Initial head conditions were set to the top of each layer for land cells and to the equivalent freshwater head for marine cells.

Convergence. The elevation of the water table was calculated as part of the model solution. Solving for the water table is strongly nonlinear, as both the groundwater flow and water table position rely on the solution of the other. This nonlinearity led to slow or no convergence for standard MODFLOW numerical solvers for our models. Thus, the steady state models were solved using MODFLOW with a Newton solver [*Niswonger et al.*, 2011], flow controlled by upstream weighting (UPW), and the "complex" option for NWT.

Multiple model complexities contributed to difficulties with model convergence. The recharge-drain boundary condition creates additional nonlinearity in the solution of the groundwater flow problem that is compounded by the solution of the water table. Also, thin model layers and sharp boundaries between high and low hydraulic conductivity units led to additional convergence challenges. The use of the Newton solver (NWT) and several hundred Newton solution iterations allowed the majority of the models to converge to less than 0.1 m of head changes between iterations and a flux change of no more than 500 m^3/day. Since the vertical accuracy of the input digital elevation model is ~2 m in relatively flat areas, this level of convergence for the water table was deemed sufficient. A maximum of 200 outer Newton iterations was allowed for model convergence. However, a few models did not converge with these initial settings (NACP: 280104; CACP: 3050208; FL: 3060204), but these models eventually converged when we increased the number of outer Newton iterations to 700, increased the flux tolerance to 1000 m^3/day, and/or forced the lowest model layer to extend to 50 m below sea-level where it otherwise did not (CACP and NACP). These models had trouble converging on a solution in inland areas of the model domain that contained steep gradients in topography combined with thin model layers that were often vertically offset.

The MODFLOW models all converged to volumetric water budget percent discrepancies of less than 0.1%, except for the Floridan 3060204 model that converged to 0.12%. The MODFLOW solution times ranged from 8 minutes to 7.7 hours, depending on the complexity and size of the models on a 64-bit Windows computer with 64 gigabytes (GB) of random access memory (RAM) and ten 2.20 gigahertz (GHz) processors for a total of twenty processing threads. Each model required approximately 6 GB of RAM for the MODFLOW model and post-processing steps.

Analysis of model results. Using the groundwater flow model results, we calculated the magnitude of groundwater discharge to coastal waterbodies and

delineated the groundwater flow paths reaching coastal waterbodies. The U.S. Geological Survey program ZONEBUDGET [*Harbaugh*, 1990] was used to calculate the groundwater budget and solve for the CGWD for each HUC8 watershed and coastal waterbody area by integrating cell-by-cell water budgets. We used the total groundwater flux from each land area to marine cells in the uppermost model layer to calculate the CGWD for that land area. To calculate the total CGWD to each coastal waterbody, we used the watersheds attached to coastal waterbodies to define individual ZONEBUDGET zones, calculated the individual CGWD contributions from each watershed to those waterbodies, and integrated those fluxes per waterbody for the total CGWD to a waterbody. This analysis is unique in that it calculates the CGWD from both the landward and seaward perspectives: the CGWD fluxes from individual watersheds to multiple waterbodies were calculated in addition to a separate calculation of the amount of CGWD reaching each coastal waterbody from multiple watersheds.

We also calculated the recharge areas contributing to CGWD using the particle tracking software MODPATH [*Pollock*, 2012]. For each active terrestrial model cell in the top model layer, four evenly distributed particles were introduced to the top face and tracked to their discharge location, either to the land surface at a terrestrial drain or to the first encountered marine cell, resulting in several million particles to track per groundwater model. At weak sinks, where only a portion of groundwater discharged to a drain, particles were allowed to continue down gradient. While some of the particles reaching weak sinks could be discharged, forcing particles to remain in the groundwater system until a full sink or a marine cell was necessary given the recharge-drain upper boundary condition and the computational limitation of only seeding four particles per topmost model cell. Backward particle tracking from the marine-land interface would require significantly more particles while potentially not capturing all of the contributing flow pathways. Only the final discharge location of the particles were recorded: initial particle tracing runs recorded full pathline trajectories but required ~15-1000 gigabytes per model, leading us to only store particle start and end locations. Areas contributing to CGWD were designated as all model cells that served as starting positions for particles discharging to a marine cell in the top model layer.

Finally, we re-ran the groundwater models and post-processing steps two additional times to assess the uncertainty in the CGWD results. For these additional runs, the recharge rates prescribed by the input raster dataset [*Reitz et al.*, 2017] were changed uniformly over each model by a factor of 0.5 (50% of the mean annual rate) and 1.5 (150%). Since the model inputs were all deterministic, including the recharge data, their uncertainty ranges were unavailable. The ±50% recharge scenarios were expected to capture the bounds of uncertainty in the steady-state recharge data, but these steady-state models do not incorporate the natural transience of recharge, which could exceed ±50% recharge for long and/or short timescales. The results of these alternate recharge models are included in the supplemental datasets for each HUC8 catchment.

Text S3. Comparison with *Sawyer et al.* [2016] and field studies

Prior to this study, *Sawyer et al.* [2016] conducted the only other study that calculated the terrestrially-sourced, fresh groundwater in a spatially continuous and distributed manner at the continental scale. Our groundwater modeling approach estimated nearly twice as much total coastal groundwater discharge for the eastern U.S. as the entirety of the U.S. coastal areas from the approach taken by *Sawyer et al.* [2016]. Despite much a much larger estimate of total groundwater fluxes, our site-specific estimates, at the watershed scale and normalized per unit length of coastline, were generally lower than the previous estimates and field sampling (Figure 2c). One source of the discrepancy between these two methods was the difference in model domain conceptualization, where *Sawyer et al.* [2016] used HUC12 catchments that were orders of magnitude smaller in area than the HUC8 catchments that were used to construct the groundwater flow model domains (Figure S4). However, the groundwater model domains were not directly constructed from the HUC8 catchments, but rather from multiple HUC8 catchments in addition to a 3 km buffer around those catchments. Additionally, the current groundwater modeling approach used particle tracking to define the contributing areas to CGWD rather than restricting the contributing areas to very small catchments along the coast with no additional groundwater flow paths from further inland (Figure S5). Thus, the current modeling approach allowed groundwater that was recharged much further inland to contribute to CGWD, whereas Sawyer et al. [2016] a priori restricted that contributing area.

Our models also predicted a much larger volume of CGWD flows into Gulf of Mexico coastal waterbodies than previously modeled for the Mississippi River Delta area [*Thompson et al.*, 2007]. *Thompson et al.* [2007] find "no groundwater with a terrestrial origin discharges" in this region while solving for salt transport in the subsurface but not the water table elevation, which was approximated as the land surface elevation. No indication of the spatial resolution of the finite-element mesh was provided, where smaller-scale coastal groundwater flow paths could have been below the resolution of their model. The coastal fluxes extracted from our numerical models integrated all terrestrially-recharge groundwater that would discharge into coastal waters and not the discharge associated with a particular location in the waterbody, but we did not solve for the freshwater-saltwater interface. However, when compared to geochemical estimates of total SGD offshore of the Atchafalaya and Mississippi River Deltas, our groundwater model predicts ~10 cm/yr of CGWD where field studies estimate between 10 to 900 cm/yr of total SGD [*Kraemer and Reid*, 1984; *Krest et al.*, 1999; *Moore and Krest*, 2004, *McCoy et al.*, 2007].

Our modeling results also consider a different scale both inland and offshore than many field studies. Field-based estimates of CGWD are often focused on nearshore areas that are likely to receive large fluxes that decay exponentially with distance offshore [*McBride and Pfannkuch*, 1975]. These nearshore field areas could be less representative of or fail to capture discharge farther offshore or for nearby portions of the coastline with different geomorphologies. Thus, our model-based estimates are lower than many field-based CGWD fluxes when compared for specific portions of the coastline (Figure 2c). Our CGWD fluxes were also generally lower than predicted by the NHDPlusV2-based fluxes where previous field data were available. However, when integrated over larger areas (i.e., catchments and waterbodies), our lower CGWD fluxes resulted in significantly larger total CGWD than the coastal NHDPlusV2-based analysis since our models could more accurately represent the total length of coastal interfaces in addition to considering cross-watershed groundwater flow [*Winter et al.*, 2003; *Schaller and Fan*, 2009].

Text S4. Model performance and explanation of Model_Performance_Summary.pdf

Groundwater level data from the U.S. Geological Survey National Water Information System (NWIS) were compared to the modeled water table for each of our model domains. The spatial extent of a model domain was used to query both the "Current Conditions" database for actively monitored groundwater sites and "Historical Observations" database for wells that are no longer monitored, referred to as "Current" and "Historic" groundwater levels, respectively. The complete time series available for each well were downloaded (complete download for all models performed on May 11, 2017), and the median hydraulic head for the time series was compared to the steady state model water table elevation for the closest model cell to the well location. Since the water table head was the target of the error analysis, only wells screened in unconfined units were needed. Thus, a well location was not included in the analysis if the aquifer type ('aq_type' column in the site data) was 'confined'. The water level data were converted to units of meters when necessary.

Two indicators of model performance were calculated with the pairs of observed and modeled groundwater levels. First, the Bravais-Pearson coefficient of determination, r^2, was calculated for each model domain for the NWIS-derived observed, O, heads and the model-predicted heads, P:

$$r^2 = \left(\frac{\sum_{i=1}^{n}(O_i - \bar{O})(P_i - \bar{P})}{\sqrt{\sum_{i=1}^{n}(O_i - \bar{O})^2}\sqrt{\sum_{i=1}^{n}(P_i - \bar{P})^2}} \right) \quad 4)$$

for n wells with the ith value representing the individual head values with the model mean values $\overline{O}$ and $\overline{P}$ [*Krause and Boyle*, 2005]. The r^2 value ranges between zero and unity, where an r^2 of zero indicates the modeled and observed heads are not correlated. An r^2 of unity indicates the dispersion of the modeled heads equals the dispersion of the observed heads, but the model predictions can still be systematically offset from the observations [*Krause and Boyle*, 2005]. Thus, the slope of the best-fit line between the observed and modeled data was calculated as a second test of the model performance. The y-intercept of the best-fit line was set to zero. A slope of unity indicates a model that yields heads close to the observed data on average. Note that no model calibration was performed to optimize the modeled heads, nor was any attempt made to filter wells based on anthropogenic modification to water levels. Thus, in densely populated areas, the modeled groundwater levels are expected to be significantly different from the median water level for the available time series due to changes in land use or groundwater abstraction/injection, and detailed analysis of well time series data was beyond the scope of the current study.

In total, nearly 15,000 current and 236,000 historic wells were used to test the performance of the models in this study, inclusive of wells used for multiple model domains. The median r^2 values for the forty groundwater models were 0.65 and 0.53 for the current and historic comparisons, respectively, with over a quarter of the models performing at 0.80 or above with each data source. The median best-fit linear slopes between the observed and modeled heads were 0.83 and 0.65 for the current and historic comparisons, respectively. An example of the model performance figures is shown in Figure S6.

For several models in different regions, the fit between the measured NWIS heads and the modeled head was affected by wells that may have been screened in confined units but not labeled as such, leading the comparison to show the model was under predicting the head where those wells were located (e.g., models CAF_2040201_fw_250m, CAF_3040201_fw_250m, and CAF_12100101_fw_250m). Similarly, models containing regions with significant anthropogenic modification of water levels are expected to primarily over-predict water table elevations.

SI References

Ator, S. W., J. M. Denver, D. E. Krantz, W. L. Newell, and S. K. Martucci (2005), A surficial hydrogeologic framework for the Mid-Atlantic Coastal Plain, *U.S. Geol. Surv. Prof. Pap.*, *1680*, 44.

Bakker, M., V. Post, C. D. Langevin, J. D. Hughes, J. T. White, J. J. Starn, and M. N. Fienen (2016), Scripting MODFLOW Model Development Using Python and FloPy, *Groundwater*, 388 doi:10.1111/gwat.12413.

Bayless, E. R., L. D. Arihood, H. W. Reeves, B. J. S. Sperl, S. L. Qi, V. E. Stipe, and A. R. Bunch (2017), Maps and Grids of Hydrogeologic Information Created from Standardized Water-Well Driller's Records of the Glaciated United States, *U.S. Geol. Surv. Sci. Investig. Report2*, *2015–5105*, 34, doi:10.3133/sir20155105.

Bokuniewicz, H. (1980), Groundwater seepage into Great South Bay, New York, *Estuar. Coast. Mar. Sci.*, *10*(4), 437–444, doi:10.1016/S0302-3524(80)80122-8.

Bokuniewicz, H., M. Pollock, J. Blum, and R. Wilson (2004), Submarine ground water discharge and salt penetration across the sea floor, *Ground Water*, *42*(7), 983–989, doi:10.1111/j.1745-6584.2004.tb02637.x.

Cambareri, T. C., and E. M. Eichner (1998), Watershed delineation and ground water discharge to a coastal embayment, *Ground Water*, *36*(4), 626–634, doi:10.1111/j.1745-6584.1998.tb02837.x.

Campbell, B. G., and A. L. Coes (2010), Groundwater Availability in the Atlantic Coastal Plain of North and South Carolina, *U.S. Geol. Surv. Prof. Pap.*, *1773*, 241.

Dalton, R. F., D. H. Monteverde, P. J. Sugarman, and R. A. Volkert (2014), *Bedrock Geologic Map of New Jersey*. Available from http://www.nj.gov/dep/njgs/pricelst/Bedrock250.pdf.

Gleeson, T., N. Moosdorf, J. Hartmann, and L. P. H. van Beek (2014), A glimpse beneath earth's surface: GLobal HYdrogeology MaPS (GLHYMPS) of permeability and porosity, *Geophys. Res. Lett.*, *41*(11), 3891–3898, doi:10.1002/2014GL059856.

Harbaugh, A. W. (1990), A computer program for calculating subregional water budgets using results from the U.S. Geological Survey modular three-dimensional ground-water flow model, *U.S. Geol. Surv. Open-File Rep.*, *90–392*, 46.

Hays, R. L., and W. J. Ullman (2007), Direct determination of total and fresh groundwater discharge and nutrient loads from a sandy beachface at low tide (Cape Henlopen, Delaware), *Limnol. Oceanogr.*, *52*(1), 240–247, doi:10.4319/lo.2007.52.1.0240.

Krause, P., and D. P. Boyle (2005), Advances in Geosciences Comparison of different efficiency criteria for hydrological model assessment, *Adv. Geosci.*, *5*(89), 89–97, doi:10.5194/adgeo-5-89-2005.

Kroeger, K. D., P. W. Swarzenski, W. J. Greenwood, and C. Reich (2007), Submarine groundwater discharge to Tampa Bay: Nutrient fluxes and biogeochemistry of the coastal aquifer, *Mar. Chem.*, *104*(1–2), 85–97, doi:10.1016/j.marchem.2006.10.012.

Maine Geological Survey (2011), Surficial Materials Maps Digital Data, Available from: http://www.maine.gov/dacf/mgs/pubs/digital/surficial_materials.zip.

Martin Jr., A., and C. D. Whiteman Jr. (1999), Hydrology of the Coastal Lowlands Aquifer System in parts of Alabama, Florida, Louisiana, and Mississippi, *U.S. Geol. Surv. Prof. Pap.*, *1416–H*, 51.

Masterson, J. P., J. P. Pope, M. N. Fienen, J. Monti Jr., M. R. Nardi, and J. S. Finkelstein (2016), Documentation of a Groundwater Flow Model Developed To Assess Groundwater Availability in the Northern Atlantic Coastal Plain Aquifer System From Long Island, New York, to North Carolina, *U.S. Geol. Surv. Sci. Investig. Rep.*, *2016–5076*, doi:10.3133/sir20165076.

Mulligan, A. E., and M. A. Charette (2006), Intercomparison of submarine groundwater discharge estimates from a sandy unconfined aquifer, *J. Hydrol.*, *327*(3–4), 411–425, doi:10.1016/j.jhydrol.2005.11.056.

Nielsen, M. G., and D. B. Locke (2015), Simulation of groundwater flow and streamflow depletion in the Branch Brook, Merriland River, and parts of the Mousam River watersheds in southern Maine, *U.S. Geol. Surv. Sci. Investig. Report*, *2014–5235*, 78, doi:10.3133/sir20145235.

Pollock, D. W. (2012), User guide for MODPATH Version 6 -- A particle-tracking model for MODFLOW, *U.S. Geol. Surv. Tech. Methods*, *6-A41*, 58.

Reay, W. G., D. L. Gallagher, and G. M. Simmons (1992), Groundwater discharge and its impact on surface water quality in a Chesapeake Bay inlet, *Water Resour. Bull.*, *28*(6), 1121–1134.

Reitz, M., Sanford, W. E., Senay, G. B., and J. Cazenas (2017), Annual estimates of recharge, quick-flow runoff, and ET for the contiguous US using empirical regression equations, 2000-2013: *U.S. Geol. Surv. Data Release*, doi:10.5066/F7PN93P0.

Resor, P. G., and J. Z. DeBoer (2005), "Hartford Basin Cross Section - Southington to Portland, CT" Guidebook for Field Trips in Connecticut, in *Guidebook no. 8*, edited by N. W. McHone and M. J. Peterson, pp. 177–189, Department of Environmental Protection, Hartford, CT.

Russoniello, C. J., C. Fernandez, J. F. Bratton, J. F. Banaszak, D. E. Krantz, A. S. Andres, L. F. Konikow, and H. A. Michael (2013), Geologic effects on groundwater salinity and discharge into an estuary, *J. Hydrol.*, *498*, 1–12, doi:10.1016/j.jhydrol.2013.05.049.

Santos, I. R., W. C. Burnett, J. Chanton, N. Dimova, and R. N. Peterson (2009), Land or ocean?: Assessing the driving forces of submarine groundwater discharge at a coastal site in the Gulf of Mexico, *J. Geophys. Res.*, *114*(C4), doi:10.1029/2008jc005038.

Sawyer, A. H., C. H. David, J. S. Famiglietti, A. H. Sawyer, C. H. David, and J. S. Famiglietti (2016), Continental patterns of submarine groundwater discharge reveal coastal vulnerabilities, *Science (80-.).*, *353*(6300), 705–707, doi:10.1126/science.aag1058.

Schlische, R. W. (1992), Structural and stratigraphic development of the Newark extensional basin, eastern North America: Evidence for the growth of the basin and its bounding structures, *Geol. Soc. Am. Bull.*, *104*(10), 1246–1263, doi:10.1130/0016-7606(1992)104<1246:SASDOT>2.3.CO;2.

Simmons, G. M. (1992), Importance of submarine groundwater discharge (SGWD) and seawater cycling to material flux across sediment/water interfaces in marine environments, *Mar. Ecol. Prog. Ser.*, *84*(2), 173–184, doi:10.3354/meps084173.

Soller, D. R., P. H. Packard, and C. P. Garrity (2012), Database for USGS Map I-1970 -- Map Showing the Thickness and Character of Quaternary Sediments in the Glaciated United States East of the Rocky Mountains, *U.S. Geol. Surv. Data Ser.*, *656*.

Thompson, C., L. Smith, and R. Maji (2007), Hydrogeological modeling of submarine groundwater discharge on the continental shelf of Louisiana, *J. Geophys. Res.*, *112*(C3), C03014, doi:10.1029/2006JC003557.

Uddameri, V., S. Singaraju, and E. A. Hernandez (2014), Impacts of sea-level rise and urbanization on groundwater availability and sustainability of coastal communities in semi-arid South Texas, *Environ. Earth Sci.*, *71*(6), 2503–2515, doi:10.1007/s12665-013-2904-z.

Williams, L. J., and J. F. Dixon (2015), Digital Surfaces and Thicknesses of Selected Hydrogeologic Units of the Floridan Aquifer System in Florida and Parts of Georgia, Alabama, and South Carolina, *U.S. Geol. Surv. Data Ser.*, *926*, 24, doi:10.3133/ds926.

Williams, L. J., and E. L. Kuniansky (2016), Revised hydrogeologic framework of the Floridan aquifer system in Florida and parts of Georgia, Alabama, and South Carolina, *U.S. Geol. Surv. Prof. Pap.*, *1807*, 140, doi:10.3133/pp1807.

Zimmermann, C. F., J. R. Montgomery, and P. R. Carlson (1985), Variability of Dissolved Reactive Phosphate Flux Rates in Nearshore Estuarine Sediments: Effects of Groundwater Flow, *Estuaries*, *8*(2), 228, doi:10.2307/1352203.

Table S1. The sub-regions of the U.S. east coast used to separate hydrogeologic provinces and summary of model input data sources.

						Source format				
Region	**Abbreviation**	**Aquifer system**	**Aquifer code***	**Models**	**Source**	**K_h**	**K_v**	**Stratigraphy**	**Layers**	**Resolution**
New England	NE	glacial origin	N100GLCIAL	8	Bayless et al. [2017]	raster	raster	raster	19	1000 m
Central Atlantic	NACP	North Atlantic Coastal Plain	S100NATLCP	5	Masterson et al. [2016]	model	model	model	20	1 mi
South Atlantic	SACP	Southeastern Atlantic Coastal Plain	S100SECSLP	7	Campbell and Coes [2010]	model	constant by layer**	model	16	1 mi
Florida, eastern Gulf of Mexico	FL	Floridan	S400FLORDN	7	Williams and Dixon [2015]	raster, constant (confining)	constant by layer	contour	5	1000 m
Central Gulf of Mexico	CGOM	coastal lowlands	S100CSLLWD	7	Martin and Whiteman [1999] Thompson et al. [2007]	constant	constant	contour	5	n/a (vector)
Western Gulf of Mexico	WGOM	coastal lowlands	S100CSLLWD	6	Martin and Whiteman [1999] Thompson et al. [2007]	constant	constant	contour	5	n/a (vector)

*Aquifer codes retrieved from http://water.usgs.gov/ogw/NatlAqCode-reflist.html

K_v values were previously calibrated for each model layer using an anisotropy ratio (K_h/K_v) within the range 1-3 [*Campbell and Coes*, 2010]

Table S2. Naming conventions used for the references of SGD field studies in Figure S3 and Figure 2c.

Short name	Reference
B1980	[*Bokuniewicz*, 1980]
R1992	[*Reay et al.*, 1992]
S1992	[*Simmons*, 1992]
Z1985	[*Zimmermann et al.*, 1985]
R2013	[*Russoniello et al.*, 2013]
M2006	[*Mulligan and Charette*, 2006]
C1998	[*Cambareri and Eichner*, 1998]
U2014	[*Uddameri et al.*, 2014]
S2009	[*Santos et al.*, 2009]
K2007	[*Kroeger et al.*, 2007]
T2007	[*Thompson et al.*, 2007]
H2007	[*Hays and Ullman*, 2007]
B2004	[*Bokuniewicz et al.*, 2004]

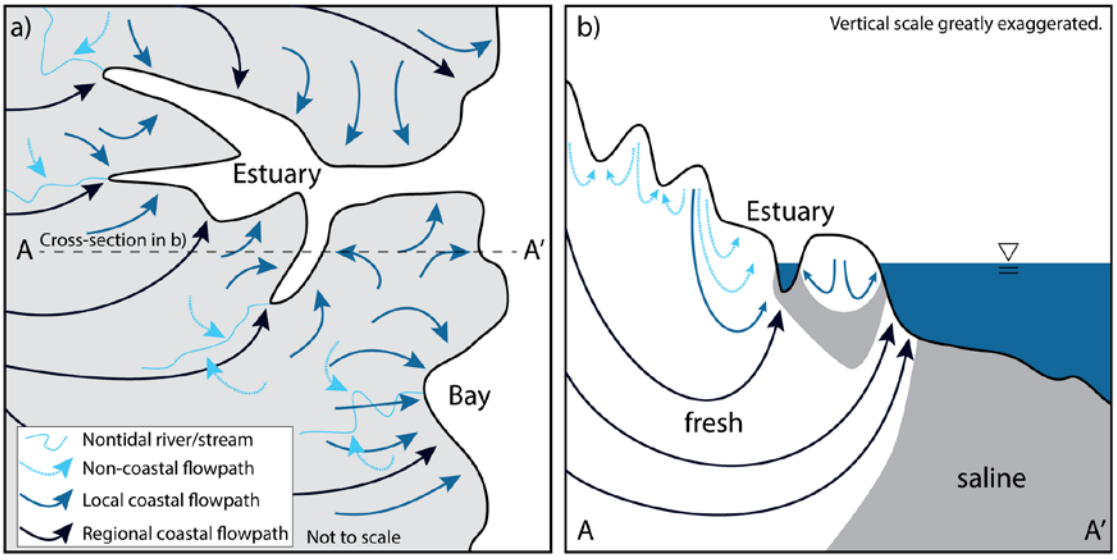

Figure S1. Hydrologic and landscape conditions combine to create complex coastal groundwater flow paths in a) map view and in b) cross-section.

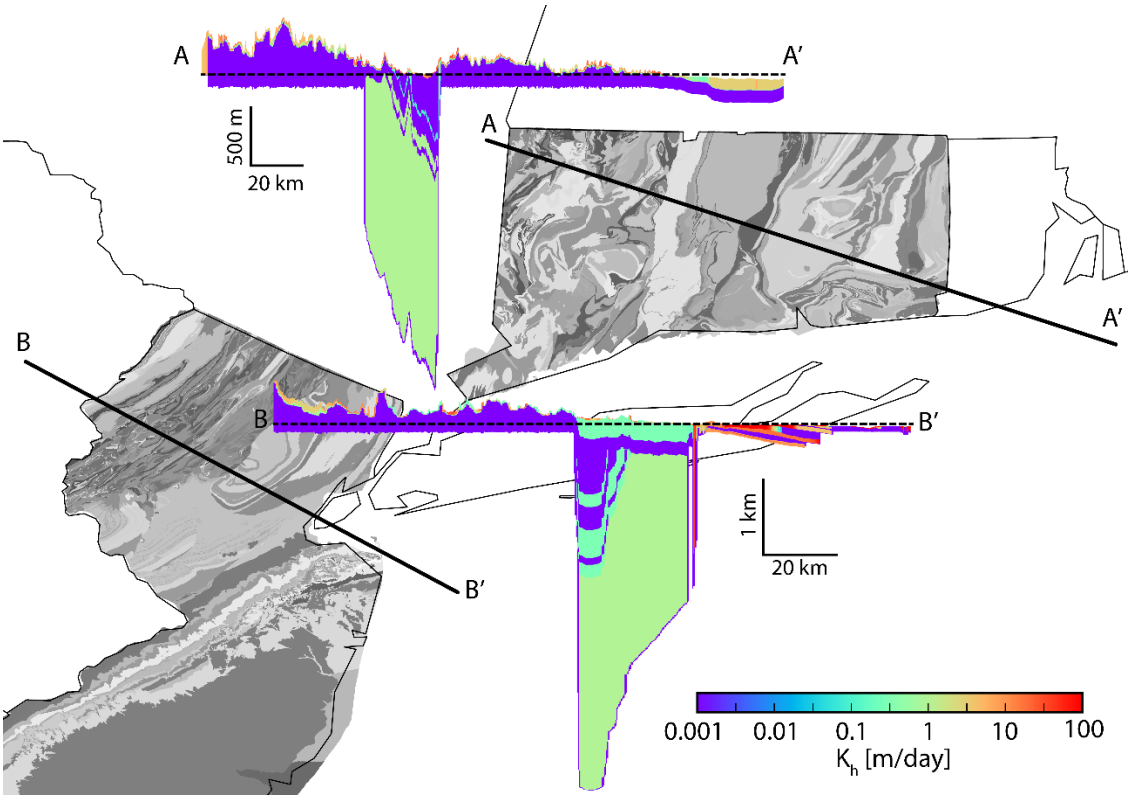

Figure S2. Model cross-sections showing stratigraphic representation of the Hartford (A-A′) and Newark Basins (B-B′). The bedrock geologies of New Jersey and Connecticut are shown in greyscale.

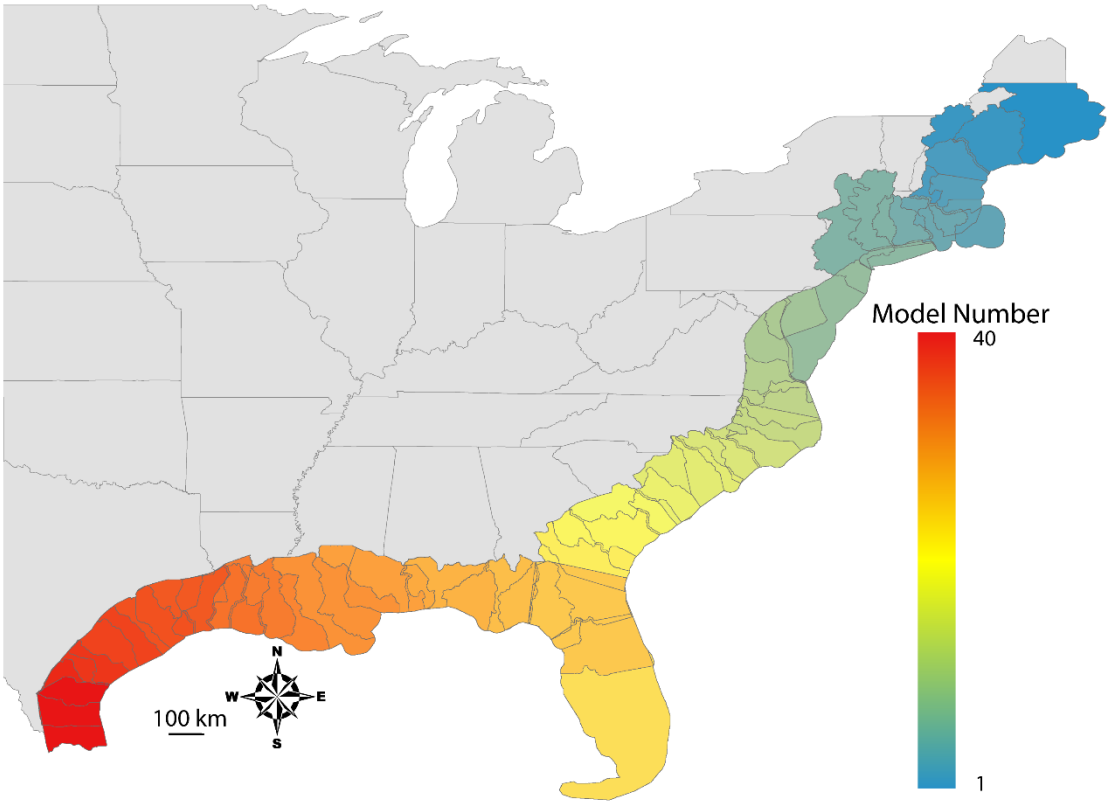

Figure S3. Model domains used in the analysis colored by model number with all model outlines in grey. For further exploration of the model domains, please refer to active_model_bounds_stats.shp in the companion dataset available at http://doi.org/10.15786/M2KG6V.

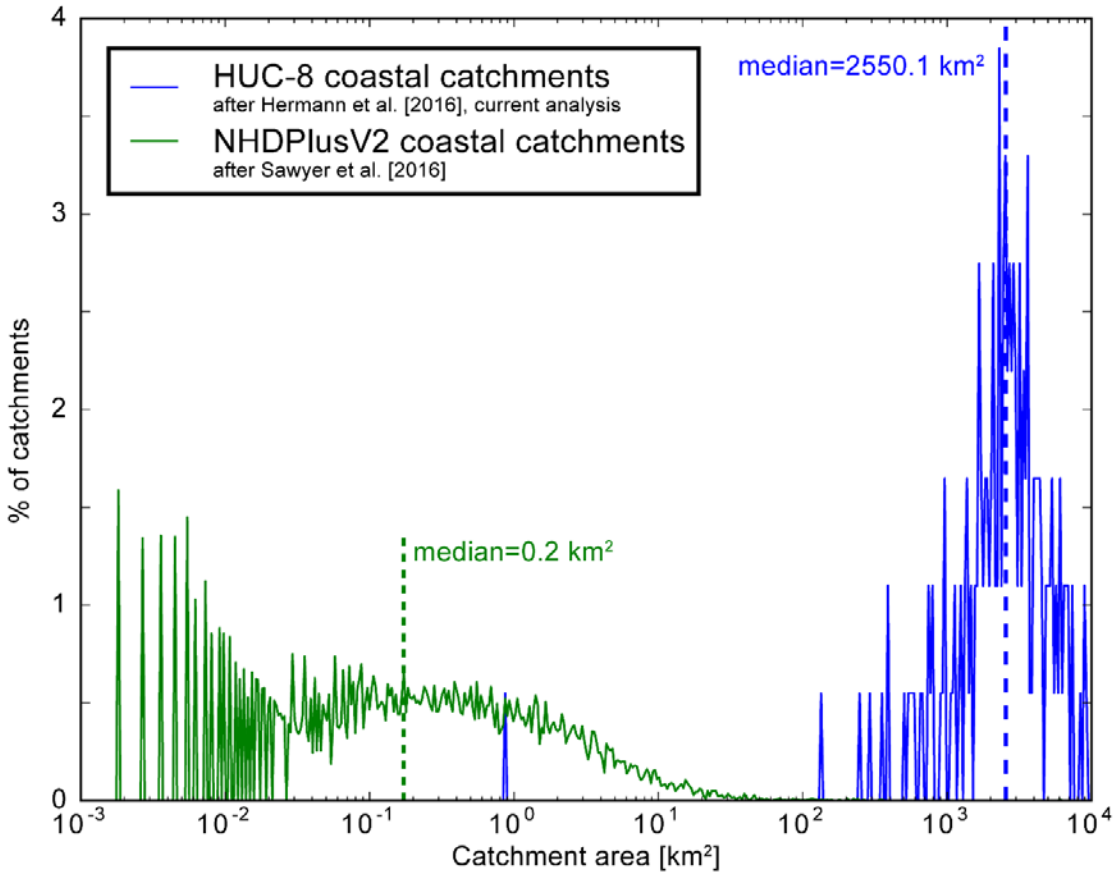

Figure S4. The NHDPlusV2 coastal catchments used in *Sawyer et al.* [2016] to estimate fresh SGD are orders of magnitude smaller than the HUC-8 catchments used in this analysis to develop the groundwater modeling domains and analyze the results.

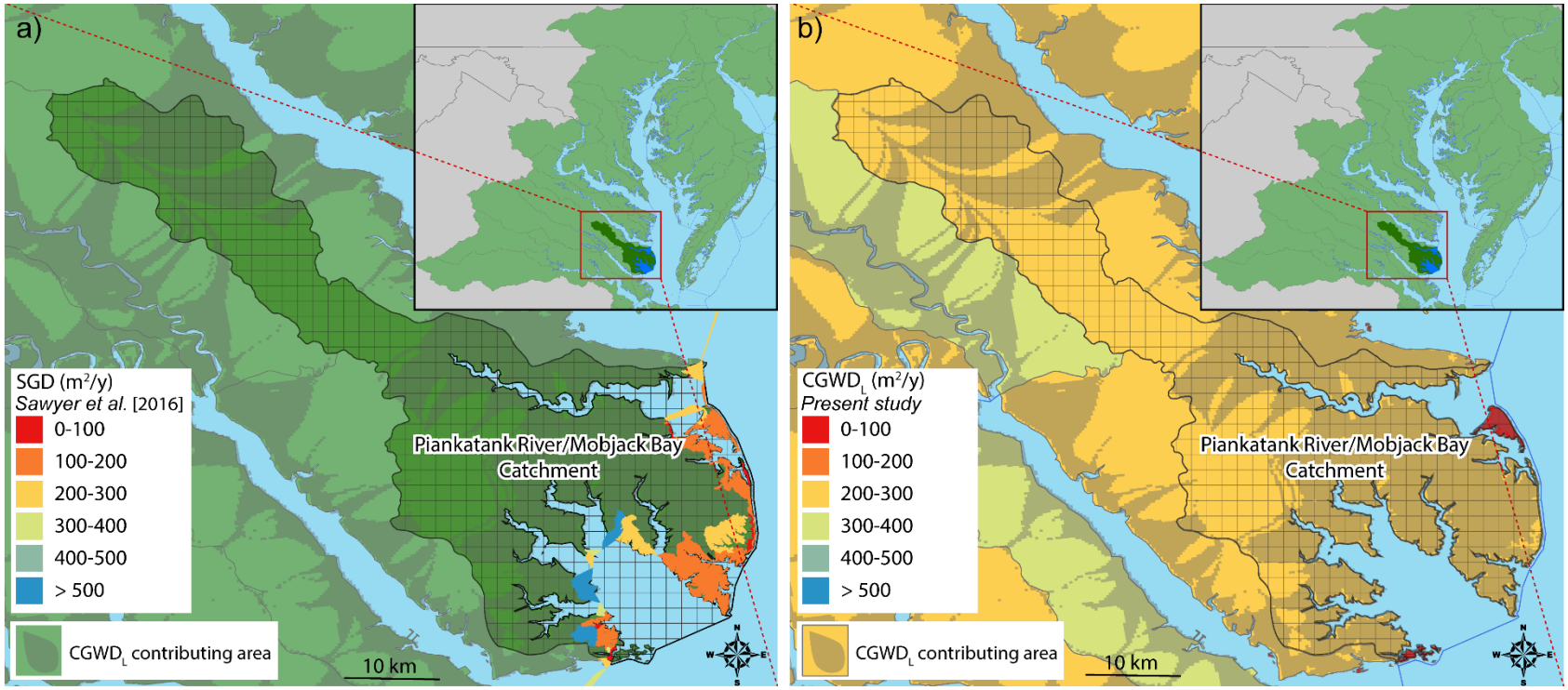

Figure S5. Comparison between coastal domains used in *Sawyer et al.* [2016] and this analysis. a)The SGD fluxes calculated from NHDPlusV2 coastal catchments in *Sawyer et al.* [2016] with a HUC-8 catchment hatched from this analysis, and b) the $CGWD_L$ calculated from the groundwater models in this analysis with the same colorbar as a). $CGWD_L$ in this analysis represents the same physical flux as SGD in *Sawyer et al.* [2016].

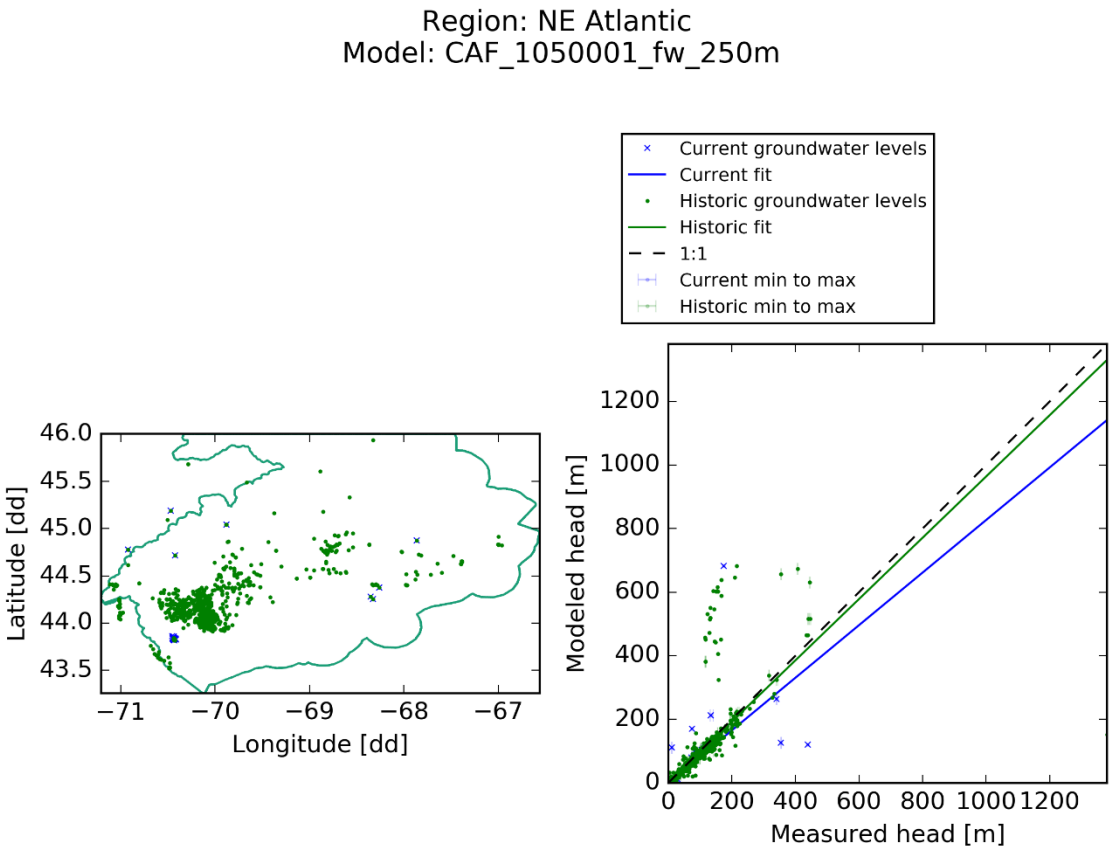

	Current	Historic
R^2	0.11	0.35
Slope_fit	0.83	0.96
N_wells	49	795

Figure S6. Example of the model performance results provided in Model_Performance_Summay.pdf for model CAF_1050001_fw_250m in the Northeast Atlantic region. On the left-hand side is a map outlining the active model area and the locations of the wells. On the right is a cross-plot of the modeled head values plotted against the measured or observed NWIS groundwater head values. R^2 is the coefficient of determination, r^2, defined in Eq. 4), and Slope_fit is the slope of the best-fit line through the data with a y-intercept of zero. The number of wells, N_wells, is provided for both the Current and Historic NWIS wells assigned not as confined aquifers. The measured head corresponds to the observation data in Eq. 4). Minimum to maximum head values for each well over the time series is shown as error bars in the x-direction ('min to max').